Paper ID ILASS08-1-4

EFFECTS OF SWIRL ON SPRAY CHARACTERISTICS OF
A COUNTER-SWIRL AIRBLAST FUEL INJECTOR

Kazuaki MATSUURA*, Syunsuke SUZUKI°, Mitsuru SUDA°, Jun IINO*, and Shigeru HAYASHI*

*Aviation Program Group, Japan Aerospace Exploration Agency, 7-44-1 Jindaiji Higashi-machi, Chofu-shi,
Tokyo 182-8522, Japan
°Faculty of Engineering, Hosei University, Kajino-cho 3-7-2, Koganei, Tokyo, Japan

ABSTRACT
The present paper discusses the effects of swirl on the spray characteristics of a counter-swirl airblast fuel injector designed for research purposes. Laser sheet imaging, laser diffraction droplet sizing and particle image velocimetry were used in the experiments whereas the gas-phase steady CFD analysis was also performed. With increasing the outer swirl angle (*OSA*), the spray angle (*SA*) increased, but more rapidly after it exceeded a threshold value. The Sauter mean diameter (*SMD*) showed its minimum roughly around this angle. The CFD results implied the importance of counter-swirl shear for good atomization. As for the effects of the inner swirl angle (*ISA*), the *SA* was larger and the *SMD* was smaller for *ISA*=-45deg. than for -60deg. For *ISA*=-20deg., the increase of the *SA* for larger *OSA* was not as rapid and the *OSA* for the *SMD* minimum was larger than the two aforementioned cases. Regarding the effects of the liquid swirl direction, the *SMD* was slightly smaller when its direction was the same as the outer air swirl than the counterpart case. The results on the injector attached with a flared outer shroud at its exit are also presented, which showed a discontinuous increase of the *SA* for the *OSA* larger than a critical angle.

INTRODUCTION

The study on the influence of injector design on the spray characteristics of aero-engine fuel injectors attracts great interest to improve combustion performance such as ignition capability, flame stability, combustion efficiency and emission performance. Since the emission regulations are getting more stringent, the conflicting requirements on emission performance such as those for oxides of nitrogen (NOx) at high power conditions and for unburned hydrocarbons (UHC) and carbon monoxide (CO) at low power conditions must be simultaneously satisfied. Thus, such a study is important to optimize the injector performance to meet the aforementioned requirements.

In aero gas turbine applications, airblast fuel injectors are widely used due to several advantages such as good air-fuel mixing [1]. In the most typical configuration of such injectors, a continuous thin annular liquid film is formed and its inner and outer sides both are exposed to the high-velocity airstreams with swirling motions so that the atomization takes place as a consequence. Such a "double swirl" airblast atomizer is of interest of the present study, and the main aim is to investigate the effect of those swirling airstreams on its atomization and dispersion characteristics.

There are literatures available relevant to the spray characterization of fuel injectors of this type, but the swirl configurations are fixed in most cases [2,3]. Some studies focusing on the effect of swirl combinations of "double-" or "multi-swirl" configurations on spray characteristics have been also carried out [4-6]. However, in most cases, investigation has been conducted for a small variation of swirl configurations so that the detailed relationship between the swirl airflows and spray characteristics has not been well clarified. In addition, some studies do not pay reasonable attention to the axial symmetry of the annular liquid film. Therefore, further study on this subject is required to obtain reliable datasets.

In this paper, we discuss the effect of swirl strength and its combination on spray characteristics of a double-swirl-type airblast injector. Here, we only focus on the "counter-swirl" configuration, where the directions of swirls of the two airstreams are opposite to each other. The reason lies on the difficulty of achieving a circumferentially uniform spray by our current injector design for the "co-swirl" configurations, especially at low liquid fuel flow rates, which may cause difficulty in data interpretation. In this paper, in addition to the swirl of air streams, the effect of liquid swirl direction with respect to the air swirl is also briefly studied. Furthermore, we also present some results on the injector attached with a flared outer shroud at its exit.

The study was carried out both experimentally and numerically. In the experimental investigation, rather simple experimental techniques were employed such as time-averaged laser sheet Mie scattering imaging and laser diffraction droplet sizing. This simple approach, compared with our previous work by means of the advanced interferometric droplet sizing technique [3,5], allows us to examine a number of swirl variations with high data production rate. In addition, for some injector configurations, two-component particle image velocimetry measurements were performed at conditions without liquid phase, mainly to understand the global airflow structure and to evaluate the numerical simulation results. With regard to the numerical simulations, Reynolds-averaged Navier-Stokes simulations for the gas-phase flow were performed to obtain three-dimensional velocity datasets. The results of numerical simulations were utilized to interpret the effect of swirl combinations on the spray characteristics obtained by the experiments.

EXPERIMENTS

Airblast fuel injector

The double-swirl airblast fuel injector used in the present study is illustrated in Fig. 1 with the definition of the coordinate. Its working principle can be found elsewhere [7], but it is briefly explained as follows. Liquid fuel is introduced to the annular fuel flow passage to form a continuous liquid film. The fuel swirl slits in the fuel flow passage give it swirl velocity component and make the annular liquid film uniform. The width of the annular fuel passage was carefully adjusted to make the annular liquid film as symmetric as possible. The liquid film is then atomized at the exit of the injector where it is sandwiched by the inner- and outer- swirling airstreams. In our design, the air and fuel flow passages are nearly parallel to the injector axis (z-axis) at the exit for simplicity. The injector has no prefilming surface so that the fuel film is exposed to both inner- and outer- air at the same time.
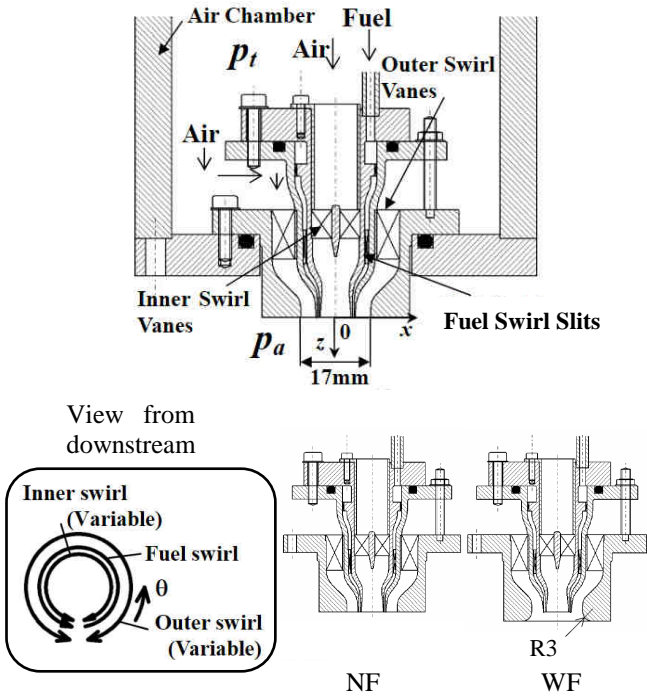

Fig.1: Schematic illustration of airblast fuel injector.

For air swirl generation, linear helical swirl vanes were employed. They were replaceable for the study of the effects of swirl combinations. A number of swirl vanes with different vane angles were prepared to finely resolve their effects on the spray. The inner swirl vane angles (*ISA*) were -60, -45, -20 and +45 deg., whereas the outer swirl vane angles (*OSA*) were -60, -45, -20, +20, +30, +45, +47, +50, +55 and +60deg. Here, the angles were defined at the mid-span position, and the positive direction of swirl is defined as anti-clockwise when looking at the injector exit from downstream. The number of blades for each swirl vane angle was determined so as to ensure the overlap between adjacent blades when viewed along z-axis to give swirl motion to the air effectively, but the manufacturing convenience was also taken into account. Thus, the number of the blades depends on the vane angles. As mentioned above, only counter-swirl combinations were studied here.

With regard to the fuel swirl, the angle of the fuel swirl slits was fixed at +45deg. Thus, in order to study the effect of the liquid swirl direction relative to the air swirl, both inner and outer air swirl vanes were replaced. For example, the inner/outer swirl vane angle combinations of both -45/+45 and +45/-45 deg. were employed. The former combination is referred to as NPP, since the directions of inner air swirl/ fuel swirl/outer air swirl is negative, positive and positive, respectively. Similarly, the latter is referred to as PPN.

In addition, we also briefly studied the spray characteristics of the injector which was attached with a flared outer shroud (simply referred to as "flare", see Fig.1) at the injector exit. The radius of the flare potion was 3mm. In this paper, the standard configuration without flare is referred to as "NF" (no-flare) and the one with flare as "WF" (with flare).

Test conditions

The experiments were conducted under atmospheric pressure, room temperature and isothermal conditions. Kerosene was used for the liquid phase to be atomized. The air pressure drop through the fuel injector normalized by the total injector-inlet pressure ($\Delta p/p_t$) was varied from 2% to 5%, whereas the air-to-fuel mass flow rate ratio (*AFR*) was varied from 3 to 15. However, since the tendency of the effects of swirl on spray characteristics was common regardless of these values [8], most of the results presented in this paper are only those for $\Delta p/p_t$=4% and *AFR*=15.

Spray and airflow characterization

The spray characterization was mainly based on the time-averaged laser sheet Mie scattering visualization and the laser diffraction droplet sizing technique.

The laser sheet visualization was utilized to characterize the global spray structure. A continuous 25mW He-Ne laser (NEC GLG570) was used as the optical source. The laser sheet was formed by a series of lenses and its thickness at the injector axis (z-axis) was 1mm approximately. The images were taken by a Nikon D80 digital camera (3872 x 2592 pixels) with a Nikon Ai Nikkor 105mm f1.8S imaging lens and a Nikon PK12 extension ring. The view area was approximately 97mm x 65 mm. The exposure time was set at 50ms to obtain sufficiently time-averaged images.

For droplet sizing, a laser diffraction spray analyzer (Tonichi Computer Applications Co. Ltd, LDSA-1500A) was employed, whose prototype was developed by one of the present authors. The relevant techniques developed for the improvement of the system performance can be found in Ref. [9]. The laser beam diameter was 5mm and the focal length and aperture of the front lens of the receiving optics was 300mm and 100mm, respectively. The quality of atomization was evaluated in terms of the Sauter mean diameter (*SMD*) at cross-sectional planes normal to z-axis, which was obtained by traversing the line-of-sight probe volume in x-direction. The cross-sectional *SMD* measurement was highly repeatable and usually the variation of the measured values for the same conditions was less than 2μm. The transmittance of the laser through the spray was more than 60% for all the conditions investigated here so that the effect of multi scattering was sufficiently small. The measurements were performed at z=10, 20, and 30mm for all cases and 50mm in addition for some cases. Nevertheless, the results only for z=30mm were presented here, since again the tendency of the effect of swirl does not change qualitatively with z position. The maximal difference of the *SMD* at z=30mm

and z=50mm was 5% through the experiments [8] (less than 2μm for $\Delta p/p_t$ =4%) and thus the atomization was regarded as almost complete at z=30mm.

For some air swirl combinations, two-component particle image velocimetry [10] measurements were also performed at conditions without liquid phase. A double pulse Nd:YAG laser at 2nd harmonic wavelength (New Wave Solo-PIV) was used as the optical source and the receiving optics consisted of an imaging lens (Nikon Ai Nikkor 105mm f1.8S) and a CCD camera (Kodak MEGAPLUS ES1.0 1000x1016 pixels). A commercial software (TSI Insight) was used for data acquisition and data processing. The laser sheet thickness was approximately 2.5mm on z-axis, and the view area was 45mm x 45mm approximately. The interrogation area employed in the PIV processing was 32 x 32 pixels, which corresponds to 1.4mm x 1.4mm at the object plane. The average velocity fields were obtained from 500 image pairs for each condition.

NUMERICAL SIMULATIONS

In order to obtain three-dimensional velocity datasets, numerical simulations based on the Reynolds-averaged Navier-Stokes Equations with the Spalart-Allmaras turbulent model [11] were performed for gas-phase flow by using a three-dimensional compressible CFD code (UPACS: Uniform Platform for Aerospace Computational Simulation) developed by the Japan Aerospace Exploration Agency [12]. Three *ISA/OSA* swirl angle combinations, -45/+20, -45/+45 and -45/+60 deg., were investigated. A sketch of the calculation domain is presented in Fig.2. The structured grid system consists of about five million grids with the smallest grid size of 0.01mm. As in Fig.2, for efficient calculations, the simulations were performed for 1/8 of the whole calculation domain with respect to the circumferential direction by enforcing periodic boundary conditions. Therefore, the number of the swirl vanes was also modified in the simulations to properly fit these periodic boundary conditions. Furthermore, as for the downstream region of the injector, a cylindrical region (like a can-type combustor), 105mm in radius and 300mm in length, were only considered instead of the infinite ambient in the experiments. The protruding portion of the injector of 36mm in diameter in Fig.1 for the better optical access in the experiments was neglected in the simulations so that the surface corresponding to the wall of the combustor dome was flat. The solid boundary condition was applied for the cylindrical wall, whereas the total pressure at the inlet of the injector and the static pressure at the exit of the cylinder were fixed through the calculation. The pressure drop was defined between these two locations in the numerical simulations, which was fixed at 4%.
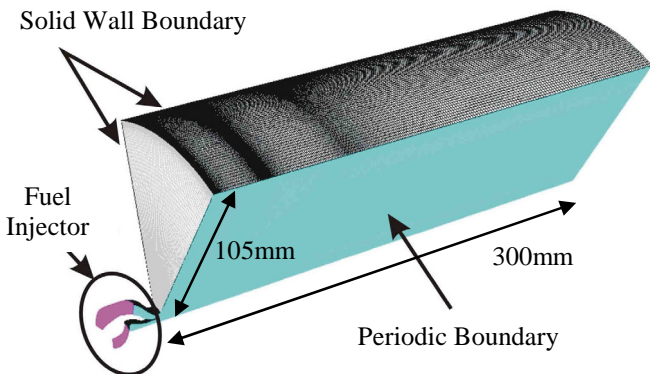

Fig.2: Sketch of numerical calculation domain.

RESULTS AND DISCUSSIONS

Brief summary on effects of air pressure drop and air-to-fuel mass flow rate ratio

Even though the present paper focuses on the effects of swirl, it is worth briefly summarizing the effects of other experimental parameters, that is, $\Delta p/p_t$ and *AFR*. In short, as $\Delta p/p_t$ increased, the *SMD* became smaller. Assuming the correlation in the form of $SMD \sim (\Delta p/p_t)^n$, n was in the range of -0.74~-1.04. The *SMD* increased as *AFR* decreased, but the effect was small for *AFR*>5. The global spray structure did not change significantly with either $\Delta p/p_t$ or *AFR*, which may be one explanation why the tendency of the effects of swirl on spray characteristics was common regardless of these values, as mentioned in the section of "Test Conditions". More details can be found in Ref. [8].

Effects of air swirl for standard injector configuration

At first, when considering the effects of the air swirl with keeping the air pressure drop across the injector the same, one important aspect is the change of air-flow rate, or in another word, the discharge coefficient. Here, the discharge coefficient is defined by the ratio of the real airflow rate to that calculated by the uniform axial velocity equal to the potential velocity at $\Delta p/p_t$ and by the area of the injector exit which is the sum of the area of the inner- and outer- airflow passages. Its dependence on the air swirl combinations for $\Delta p/p_t$ =4% in the absence of spray is presented in Fig.3. It also changes depending on $\Delta p/p_t$, but the variation is less than 7% and the trends are similar. The figure also includes the CFD results for *ISA*=-45deg., which will be discussed later. The discharge coefficient or the airflow rate decrease as either *ISA* or *OSA* increases. It changes in a wide range between 0.49 and 0.73. It should be noted that the fuel flow rate was also adjusted when swirl angles were varied in order to compare the results at the same *AFR* conditions.

The effects of air-swirl combinations on the spatial spray patterns, spray angle (*SA*) just after the injector exit, and the *SMD* at z=30mm are presented in Figs. 4, 5, and 6, respectively. They are only for $\Delta p/p_t$=4% and *AFR*=15, but again, the tendency discussed below is common for the other conditions. For *OSA*=+20, +45 and +60deg., PIV measurements were also performed without liquid phase and the results for $\Delta p/p_t$=4% are shown in Fig. 7.
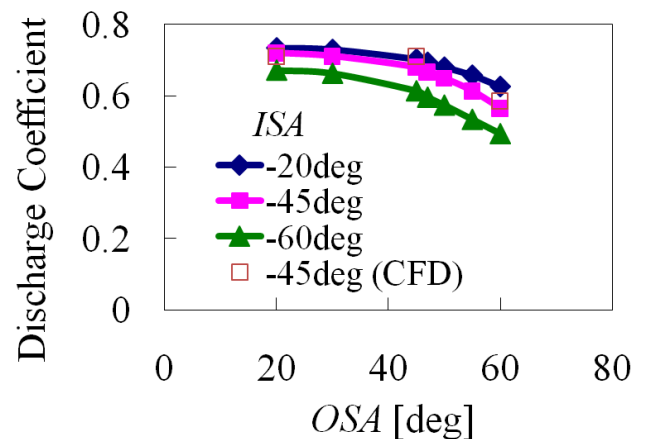

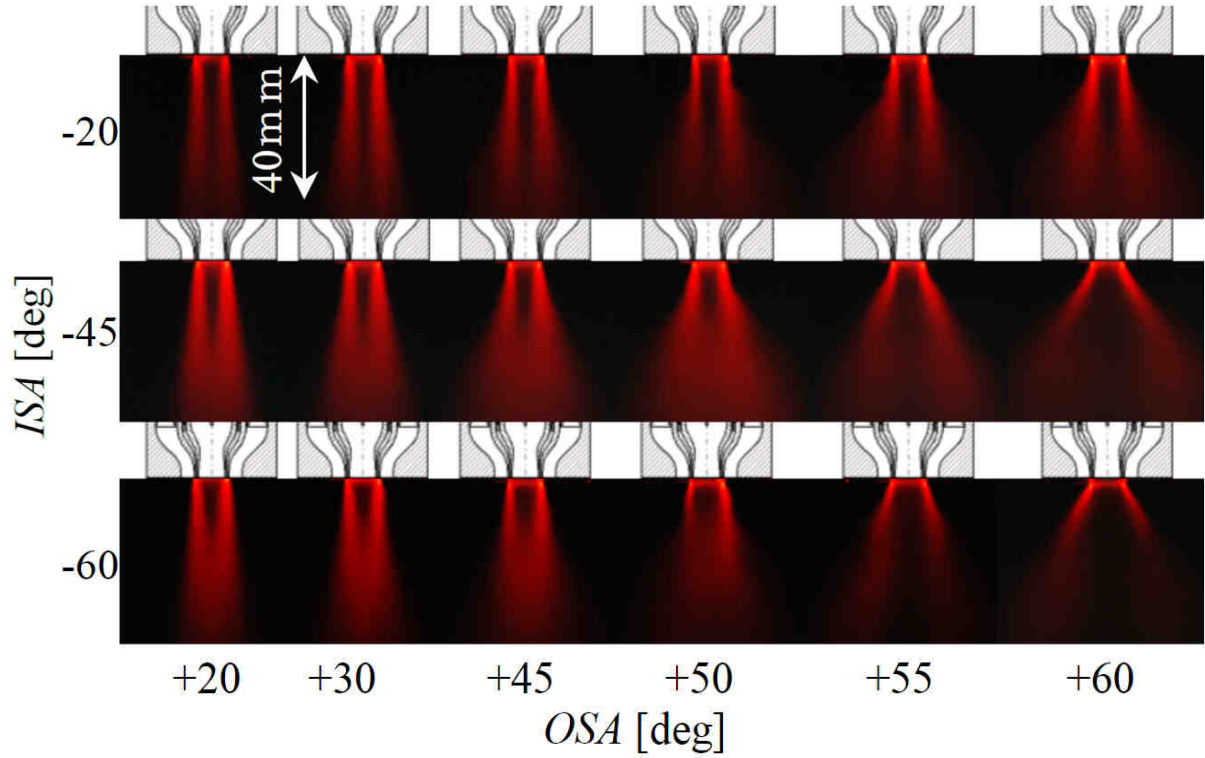Fig.3: Airflow discharge coefficients with different air-swirl combinations ($\Delta p/p_t$ =4%).

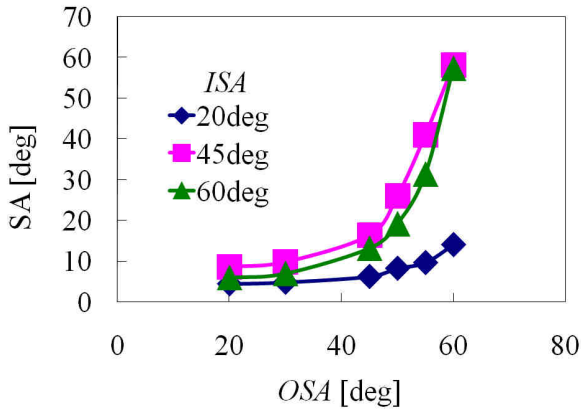Fig.4: Time-averaged laser-sheet Mie scattering images ($\Delta p/p_t$ =4%, AFR=15).

Fig.5: Effect of swirl combinations on spray angles at the injector exit ($\Delta p/p_t$ =4%, AFR=15).
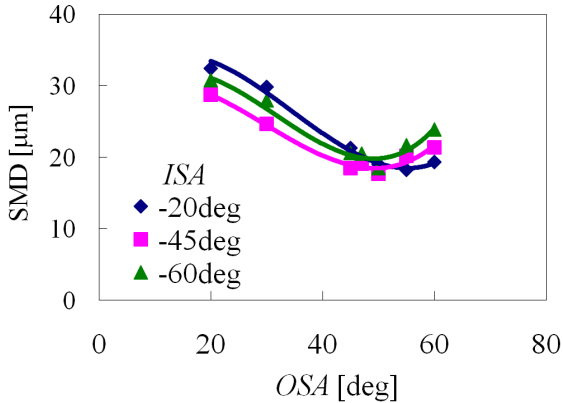

Fig.6: Effect of swirl combinations on SMD ($\Delta p/p_t$=4%, AFR=15, z=30mm).

Firstly, the spray angles increase as the OSA increases, as observed in Figs. 4 and 5. They especially show a rapid increase after the OSA exceeds a threshold value. This value is roughly about +45deg. for ISA=-45 and -60deg. This rapid increase may be mainly due to the change of airflow field itself as seen in Fig.7. For example, for ISA=-45deg., the airflow spreads much wider for OSA=+60deg. than for OSA=+45deg., and a wide central recirculation zone is observed for the former case. For ISA=-20deg., the curve in Fig.5 deviates from the other two. However, the slope of the curve for the larger OSA (larger than +50deg., approximately) is again relatively steeper than for the smaller OSA, though the change of the slope is not as distinctive. On the other hand, for the same OSA, the SA shows the largest value at ISA=-45deg. among the three ISA cases. The reason is possibly explained as follows. For ISA=-20deg., the centrifugal effect of the inner air is small and the relatively higher axial momentum of this low swirl jet is given to the liquid phase through the two-phase interaction. Even for the high outer-swirl cases, the central low-swirl high-speed jet does not allow the outer air to spread as typically seen in Fig. 7 for ISA/OSA=-20/+60 deg., in order to satisfy the continuity of the fluid. Thus, the spray does not spread out as easily as it does for ISA=-45deg. On the other hand, for ISA=-60deg., the strong swirl results in the generation of the central low-speed zone or recirculation zone, but because of the strong shear of the counter swirl motion, both inner and outer swirl decays quickly. This causes the zone to be closed narrow and short [13], and the flow is induced inside as the zone closes downstream. This eventually results in narrower spreading of both the airflow and the spray than for ISA=-45deg.

It is also interesting to note that more droplets are distributed in the central region downstream (z>20mm) for larger ISA and smaller OSA. One possible reason is the more enhanced local turbulence due to the strong shear and/or the deceleration of flow in this region which give droplets longer residence time to spread by turbulent motion. Also, local vectors directing inward in this region are also observed, which may be another reason.
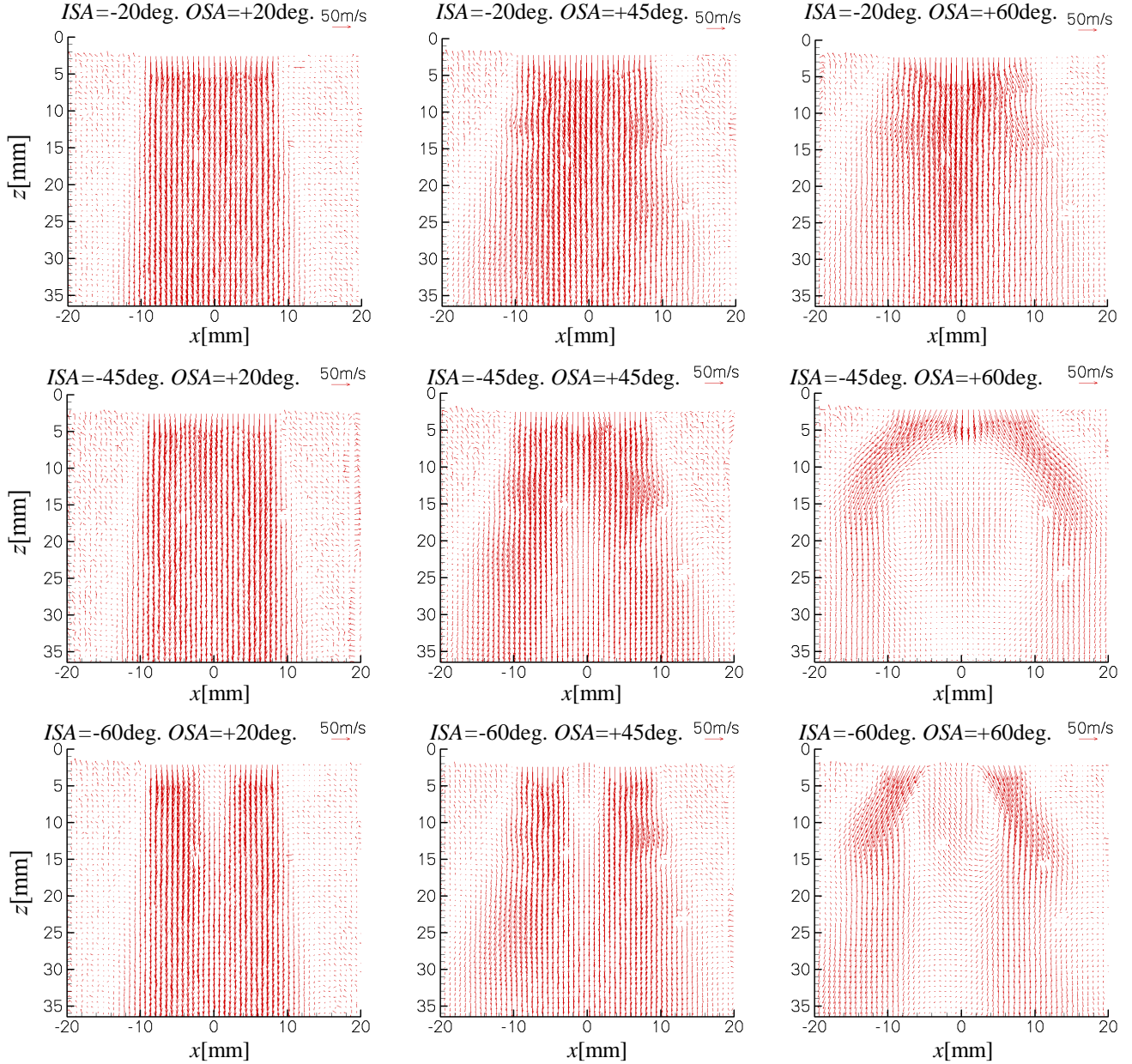
Fig.7: Mean velocity vector plots in *zx*-plane obtained by PIV measurements ($\Delta p/p_t$=4%).

Concerning the droplet size, at a fixed value of *ISA*, the *SMD* shows its minimum at *OSA*=+50deg. approximately, for *ISA* =-45 and -60deg. This is also true for *ISA*=-20deg., despite the shift of the minimum to *OSA* = +55deg. The smaller *SMD* for the larger *OSA* on the left side of the minimum is possibly due to the more pronounced shear of the counter-swirl boundary layer. On the other hand, as for the reason for the larger *SMD* for the larger *OSA* on the right side of the minimum, following the interpretation of Aigner and Witting [4], we could point out the lower shear stress on the inner wall of the outer air passage for the larger *OSA* resulting from the larger centrifuging effect of the outer air. However, since our injector has the contraction of the outer airflow passage close to the exit which their injectors in Ref. [4] did not have, it is not clear if this is the main cause in our cases. On the other hand, here, it is interesting to note that the *OSA* at the *SMD* minimum almost coincides or at least well correlated with the value at which the slope of the *SA* against the *OSA* begins to show the rapid increase. Thus, the rapid spreading of the airflow for the larger *OSA* on the right side of the minimum seems to affect the quality of atomization.

One possible reason is the deceleration of the airflow for the larger *OSA*. This effect will be discussed further with CFD results later.

On the other hand, for a fixed *OSA*, the *SMD* shows smallest values for *ISA*=-45deg. among the three in the range of small *OSA*, whereas it does for *ISA*=-20deg. in the range of large *OSA*. Focusing on the comparison between the results of *ISA*=-20 and -45deg., the reason for the smaller *SMD* for *ISA*=-45deg. is possibly again due to the more intense shear. The inverse relationship for the larger *OSA* could be explained by the deterioration of atomization quality for *ISA*=-45deg. in this *OSA* range. As for *ISA*=-60deg, the trend of the curve in Fig. 6 is similar to that for *ISA*=-45deg., but the *SMD* shows the larger values. The reason for this has not been currently clarified and further investigation including CFD analysis is ongoing.

As discussed, the circumferential shear layer seems to play an important role in atomization process. On the other hand, the PIV results in Fig.7 are those of two-component velocity vectors. Therefore, for better understanding, the CFD results are employed in the following. Firstly, the degree of agreement

between the results of the CFD and the experiments are briefly discussed. The CFD global velocity vector field structures in the *zx*-plane (not shown in this paper) were in good agreement with those by PIV for all the cases for which the CFD was performed, and the difference of the discharge coefficients in Fig.3 between the CFD and the experiments was 4.3% at maximum. Examples of radial distributions of axial and radial velocity components are presented in Fig. 8 for detailed comparison. Here, the CFD results are those averaged in the circumferential direction. The results are not simply compared because of the simplification of CFD boundary conditions including the modified number of the swirl vanes. In Fig.8, some discrepancy is observed, which could be partly due to the difference of the boundary conditions. The CFD results reasonably predict qualitative characteristics, whereas the care should be taken on quantitative interpretation.
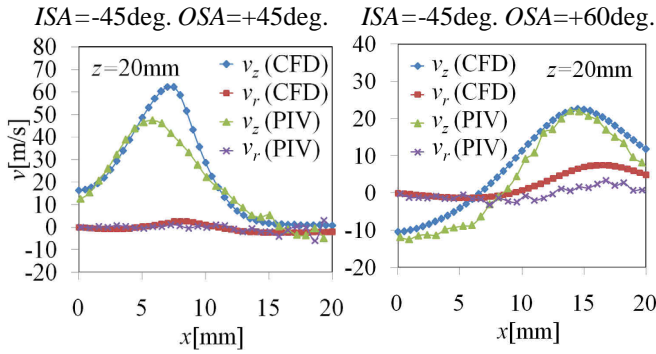

Fig.8: Comparison between radial distributions of mean axial and radial velocities obtained by CFD and PIV ($\Delta p/p_t$=4%).

The radial distributions of the absolute, axial, radial and circumferential velocities (v_a, v_z, v_r and v_θ, respectively) are plotted together with those of Mie scattering intensity I_M for the three cases with *ISA*=-45deg. in Fig.9, at *z*=2mm and 10mm. Some parts of the I_M curves are clipped because of the saturation of the CCD, but this does not affect qualitative identification the liquid phase location. For *OSA*=+20 and +45deg., the values of v_a are similar for both *z* positions, whereas v_θ shows large difference in the region of the outer airflow. These results imply that the *SMD* difference between the two cases is not due to the magnitude of v_a but due to the strength of the circumferential shear. On the other hand, for *OSA*=+60deg., v_a for the inner air at *z*=2mm is smaller than the other two, despite the same *ISA*. This is due to the wider spreading of the airflow and the existence of the recirculation zone, which is associated with the stronger positive pressure gradient and flow deceleration. Because of this spreading effect, despite the larger *OSA*, the "overall" shear intensity in the region where the liquid phase is distributed is even lower than for *OSA*=+45deg. at this upstream position already. This tendency is more pronounced at the downstream position (*z*=10mm). This could be a possible explanation of the *SMD* minimum as discussed above, provided that the shear intensity is the dominant factor in the atomization process of the present injector. On the other hand, the magnitude of v_a of the outer air is similar to the other two at *z*=2mm, which is also true for *z*=0mm (not shown). From the distribution of v_a, the less wall shear stress of the outer air in Ref. [4] does not seem the dominant reason for the larger *SMD* for *OSA*=+60deg. than +45deg. in the present cases. As for the reason for the smaller *SMD* for *OSA*=+60deg. than +20deg., this is possibly because of the stronger shear at upstream region and/or because of the region of almost no circumferential shear near the outer edge of

the spray for *OSA*=+20deg. However, it should be mentioned that detailed quantitative explanation probably cannot be given by the present single-phase simulation results.
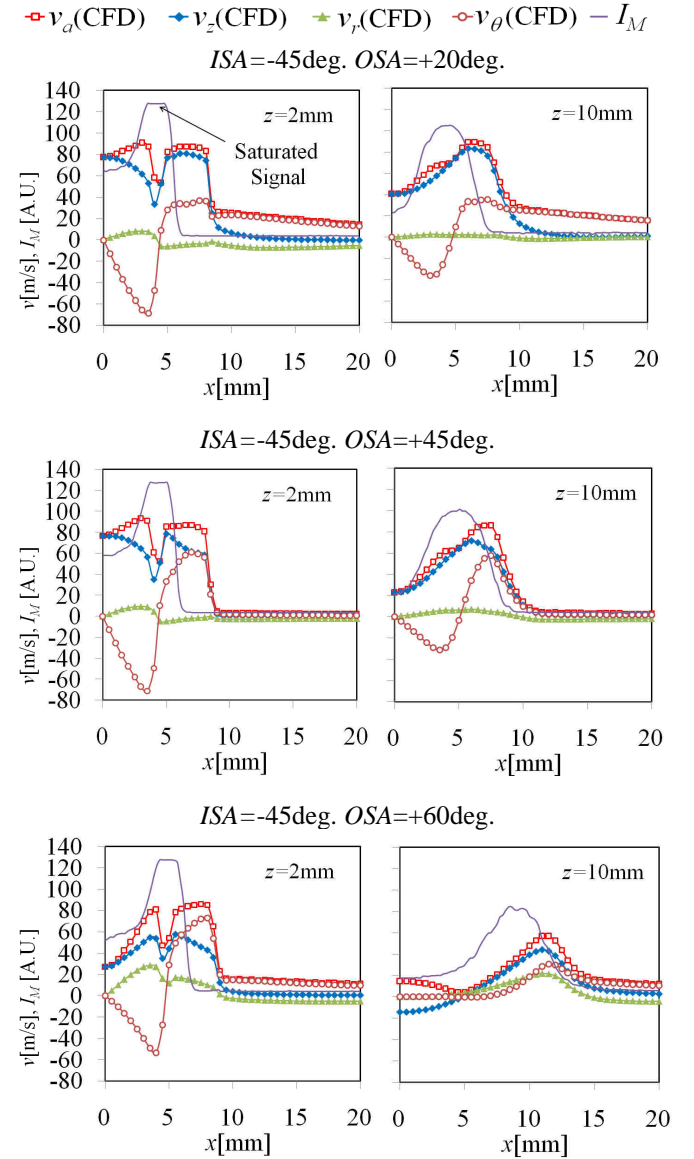

Fig.9: Radial distributions of mean velocity components by CFD and Mie scattering intensity ($\Delta p/p_t$=4%).

Effects of liquid swirl direction for standard injector configuration

The effect of liquid swirl direction on the *SMD* are presented in Fig.10 for inner/outer swirl vane angle combinations of -45/+45 deg. (NPP) and of +45/-45 deg. (PPN). As mentioned, the fuel slit angle is fixed at +45deg. The NPP combination results in slightly better atomization than the PPN. This tendency is generally observed for different *AFR* and swirl vane angles. Despite the small *SMD* difference, the measured *SMD* and its tendency with respect to the NPP and PPN are highly repeatable. On the other hand, the global spray dispersion patterns from the laser sheet Mie-scattering images are almost identical. Thus, though the degree of the improvement of atomization is small, this characteristic might be useful from the practical fuel injector designing point of view.
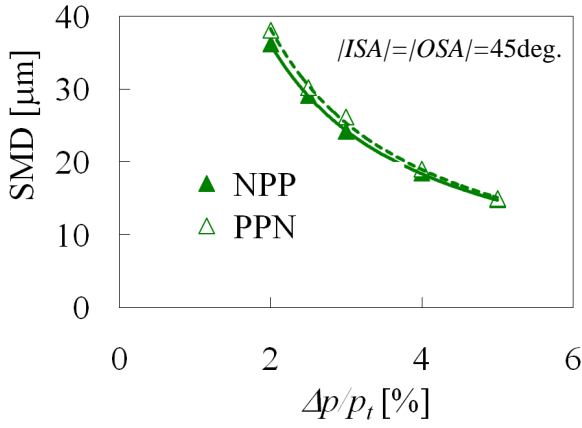
Fig.10: Effect of air- and liquid-swirl combinations on SMD ($|ISA|=|OSA|=45$deg., $\Delta p/p_t=4\%$, $AFR=15$, $z=30$mm)

The reason for the SMD difference is not clear and further investigation is required. However, the backlight photograph of the PPN in Ref. [8] shows local streaks of the liquid film, which were hardly observed if long exposure times were employed. These streaks are relatively more evident than those of the NPP [8]. Thus, this may probably cause the generation of large droplets locally which results in the larger SMD.

Injector with flare

The results of the injector with the flare are discussed in this section. The effects of air-swirl combination on the spatial spray patterns, SA, and SMD at $z=30$mm are shown in Figs.11, 12, and 13, respectively, for $\Delta p/p_t=4\%$, $AFR=15$ and $ISA=-45$deg.

With increasing the OSA, the spray structure changed remarkably at a critical outer-swirl angle of $+50$deg., as seen in Fig.11. At this critical angle, two different spray structures were observed which switch from one to the other by an artificially enforced large flow disturbance as a trigger, for example, by momentarily inserting a block into the flow. However, both modes were stable in the absence of such a disturbance. The reason for this remarkable change below and above $OSA=+50$deg. was due to the change of airflow structure depending on the strength of outer air swirl. In the beginning, the outer air flows along the flare wall with the help of the Coanda effect and thus turns outward, but along the way to the injector exit, flow separation takes place for the smaller OSA because of the quick expansion of the flare passage. Therefore, the air spreads modestly. On the other hand, for the larger OSA than the critical value, the strong swirl allows the air to attach to the wall surface so that the air flows along the flared wall all the way and the airflow drastically spreads outward.
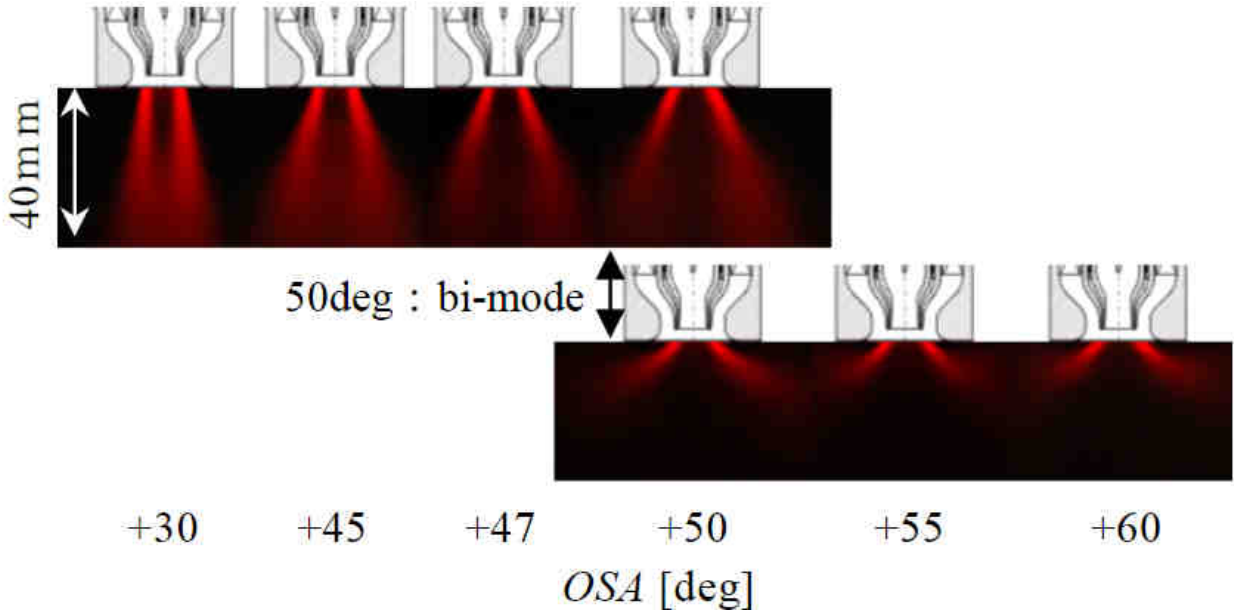

Fig.11: Time-averaged laser-sheet Mie scattering images for injector with flare ($ISA=-45$deg., $\Delta p/p_t=4\%$, $AFR=15$).
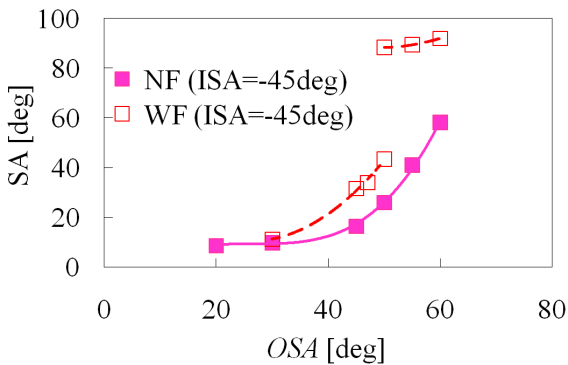

Fig.12: Effect of flare on spray angles at the injector exit ($ISA=-45$deg., $\Delta p/p_t=4\%$, $AFR=15$, $z=30$mm).

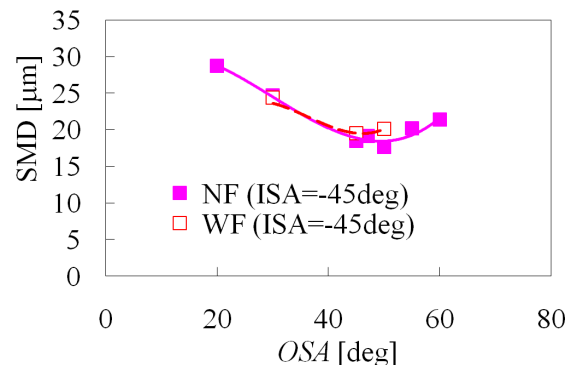Fig.13: Effect of flare on SMD ($ISA=-45$deg., $\Delta p/p_t=4\%$, $AFR=15$, $z=30$mm, for modest spreading mode).

The results of the *SA* for the configuration with the flare (WF) are compared with those for the standard configuration (no-flare, NF) in Fig.12. The data plotted for the NF are the same as those used in Fig.5. In case of the WF, the *SA* again increases as the *OSA* increases similar to the NF case, but the values for the WF are larger, for the *OSA* between +30 to +50deg. as expected. For the *OSA* larger than the critical angle +50deg., it becomes significantly large, but after that its dependence on the *OSA* is relatively modest.

Droplet size measurements were performed only for the *OSA* smaller than or equal to +50deg. with the modest spreading mode (upper row in Fig.11) and the results are presented in Fig.13. For the *OSA* larger than +50deg., spray measurements were not straight forward because of the fouling problems of the optics by spray droplets. The *SMD* for the WF shows a similar tendency to the NF with respect to the *OSA*. Also, the difference of the *SMD* values between the two is not significant, though the *OSA* at the smallest *SMD* shifts slightly to a smaller value for the WF. The reason for the modest *SMD* change despite the large *SA* difference is not clear at this stage and further investigation including CFD analysis is ongoing.

CONCLUSIONS

The effects of swirl on the spray characteristics of a counter-swirl airblast fuel injector were investigated. Time-averaged laser sheet Mie scattering imaging, laser diffraction droplet sizing and particle image velocimetry (PIV) were used in the experimental study. The CFD analysis based on the Reynolds-averaged Navier-Stokes equations with the Spalart-Allmaras turbulent model was performed to solve the gas phase flow for better interpretation of the experimental data. The velocity fields obtained by PIV and CFD were reasonably in good agreement. The conclusions are as follows.

With increasing the outer swirl angle (*OSA*), the spray angle (*SA*) increased, but more rapidly after it exceeded a threshold value, which depended on the inner swirl angle (*ISA*). The Sauter mean diameter (*SMD*) showed its minimum roughly around this angle with respect to the change of the *OSA*. The strength of the counter-swirl shear seemed to be important for good atomization, but it was not a monotonic function of the *OSA* because wider spreading of the airflow for larger *OSA* caused less intense shear layer which is already the case just slightly downstream of the injector exit. This could be considered as the cause of the *SMD* minimum and its correlation with the rapid increase of the *SA*.

The effect of the *ISA* also depended on the *OSA*, but for *ISA*=-45 and -60deg., it showed similar behaviour in terms of the relationship of the *OSA* with the *SA* and *SMD*. The *SA* was larger and the *SMD* was smaller for *ISA*=-45deg. For *ISA*=-20deg., the increase of the *SA* for larger *OSA* was not as rapid and the *OSA* for the *SMD* minimum was larger than the other two cases.

The effect of liquid swirl direction was also studied for the counter-swirl air combinations. The *SMD* was slightly smaller for the case that the liquid swirl direction was the same as the outer air swirl than the counterpart case, which is possibly due to the better uniformity of the liquid film but the reason was not sufficiently clear at this stage.

Furthermore, the spray from the injector attached with a flared outer shroud at its exit was also investigated for *ISA*=-45deg. For the *OSA* larger than +50deg., the spray structure showed significantly wide spreading. At this critical angle, two different spray structures were observed which switched from one to the other by an artificially enforced large

flow disturbance, but both modes were stable in the absence of such a disturbance. For the cases of the relatively modest spreading mode, the dependence of the *SA* on the *OSA* showed similar tendency to those without the flare, though the values were larger. The *SMD* values were similar between the two injector configurations despite the difference of the *SA*.

ACKNOWLEDGMENT

REFERENCES

[1] A. H. Lefebvre, Airblast Atomization, *Prog. Energy Combust. Sci.*, vol. 6, pp. 233-261, 1980.

[2] Q. P. Zheng, A. K. Jasuja and A. H. Lefebvre, Structure of Airblast Sprays under High Ambient Pressure Conditions, *ASME 96-GT-131*, 1996.

[3] K. Matsuura, K. Zarogoulidis, Y. Hardalupas, A. M. K. P. Taylor, T. Kawaguchi, D. Sugimoto and K. Hishida, Simultaneous Planar Measurement of Size and Three-Component Velocity of Droplets in an Aero-Engine Airblast Fuel Spray by Stereoscopic Interferometric Laser Imaging Technique, *Proc. 10th ICLASS 2006*, Paper No. 06-240, 2006.

[4] M. Aigner and S. Wittig, Swirl and Counterswirl Effects in Prefilming Airblast Atomizers, *ASME 87-GT-204*, 1987.

[5] K. Matsuura and Y. Kurosawa, Effect of Swirl Combinations on Spray Dispersion Characteristics of a Multi-Swirler Airblast Atomizer, *Proc. 20th ILASS-Europe 2005*, pp. 355-360, 2005.

[6] S. Miyamoto, M. Mikami, N. Kojima, A. Fujii and T. Saito, Spray Characteristics of LPP Gas Turbine Injector -An Experimental Study on Optimum Swirler Condition-, *Proc. 10th ICLASS 2006*, Paper No. 06-133, 2006.

[7] A. H. Lefebvre, Atomization and Sprays, Hemisphere Pub., 1988.

[8] S. Suzuki, M. Suda, K. Matsuura and S. Hayashi, Effects of Design Parameters and Operating Conditions on Spray Characteristics of Annular-Liquid-Film-Type Airblast Atomizers -Second Report: Effects of Swirl Angles-, *JAXA RM*, 2008 (in Japanese, to be submitted).

[9] S. Hayashi, Measurements of Absolute Concentration and Size Distribution of Particles by Laser Small Angle Scattering, in G. Gouesbet and G. Grehan (eds), *Optical Particle Sizing, Theory and Practice*, p.549, Plenum Press, 1987.

[10] M. Raffel, C.Willert, J. Kompenhans, Particle Image Velocimetry: A Practical Guide, Springer, 1998.

[11] T. Yamane, K. Yamamoto, S. Enomoto, H. Yamazaki, R. Takaki and T. Iwamiya, Development of a Common CFD Platform - UPACS -, *in Parallel Computational Fulid Dynamics - Proceedings of the Parallel CFD 2000 Conference, Trondheim, Norway*, Elsevier Science B. V., pp. 257-264, 2001.

[12] P. R. Sparlart and S. R. Allmaras, A one-equation turbulence model for aerodynamic flows, *AIAA Paper 92-0439*, 1992.

[13] K. Merkle, H. Büchner, N. Zarzalis, and O. N. Sara, Influence of Co and Counter Swirl on Lean Stability Limits of an Airblast Nozzle, *ASME GT2003-38004*, 2003.